Efficient Programmable Pulse Shaping for *X*-Band GaN MMIC Radar Power Amplifiers

Corrado Florian, *Member, IEEE*, Tommaso Cappello, *Graduate Student Member, IEEE*, Daniel Niessen, *Member, IEEE*, Rudi Paolo Paganelli, Scott Schafer, *Student Member, IEEE*, and Zoya Popović, *Fellow, IEEE*

***Abstract*— This paper presents a supply modulated *X*-band 12-W peak power transmitter that maintains an average efficiency greater than 50% for various shapes of amplitude-modulated pulses. The main power amplifier is a two-stage GaN-on-SiC MMIC with a peak efficiency of 65%, while the pulse envelope modulator is a 95% efficient hybrid 3-b power DAC implemented with GaN-on-Si transistor switches. Envelope shaping of a pulsed waveform results in improved spectral confinement of greater than 15 dB for the first sideband compared with constant-envelope pulses, with over 20 points improvement in total efficiency. The combination of supply modulation and digital predistortion is shown to result in high composite (total) efficiency of over 55%, with simultaneous high dynamic range and with flexible digitally programmable pulse shaping.**

***Index Terms*— Envelope tracking (ET), power DAC (pDAC), radar pulse shaping, spectral confinement, supply modulator.**

I. Introduction

THE majority of radar systems operate the high power amplifier (PA) of the transmitter in pulsed regime: the characteristics of the RF/microwave pulses in terms of duty cycle, pulsewidth, repetition frequency, transmitted power, and pulse shaping directly affect radar performance [1]. Solid-state phased array radar is enabled by a large number of transmit modules that produce very high transmit powers. A typical transmit module has an efficient nonlinear deep class-AB to class-C PA that transmits constant-envelope pulses with significant spectral content over a large bandwidth [1]. Advanced radar waveforms can be used to provide spectral confinement, improve range ambiguity, and decrease detectability for active electronically scanned arrays [2]. In search and tracking radar, target detection and identity discrimination can be improved [3], while in weather radar suppression of transmitted spectral sidebands enhances performance [4]. In addition, there is increased concern about radar spectral emissions interfering with communication spectrum allocations [5].

Amplitude modulation of the envelope provides spectral confinement effects on radar system performance for different envelope shapes [1]–[7]. The amplitude-modulated pulse can be provided at the input of the PA while the supply voltage is kept constant over the pulse duration. Such drive-modulated PAs operate in backoff at lower amplitudes, resulting in significant average efficiency degradation. In [6] and [7], an outphasing PA with a Gaussian envelope shape, with up to a 3-dB peak-to-average ratio (PAR) waveform, is experimentally investigated, but the average system efficiency is not reported.

More recently, supply modulation (SM) was introduced as a means to amplify amplitude-modulated pulses without sacrificing PA efficiency [8]–[16]. Various types of SM following up on the early envelope elimination and restoration (EER) technique [17] have been applied to improve efficiency of transmitters for high peak-to-average power ratio (PAPR) communication signals [8]–[13]. In [2], a pulsewidth modulation (PWM) 100-MHz switching converter is used for linear pulse shaping of an integrated *S*-band PA, with a total efficiency of 27%. For pulse shaping of a hybrid *S*-band GaN PA in [14], a variable supply [15] is implemented as a simple damped resonant circuit with efficiency greater than 90% at 6-W output power and a total efficiency 50% and greater than 65% for the PAPR values of 8 and 4 dB, respectively. An average 66% total efficiency was demonstrated for a Blackman-window pulse with a 4.1-dB PAPR and −30-dB spectral sidelobe levels. In [15] and [16], this method was applied to *X*-band GaN PAs with variable 7–15-μs pulsewidths and a resulting efficiency of 40%. For good sideband suppression, simple predistortion of the PA gain and phase was required in this approach. Although good efficiency improvement and spectral confinement were demonstrated, the drawback of the technique is that it is limited to a single pulse shape due to the resonant nature of the supply.

In this paper, we extend the supply pulse shaping technique to a fully programmable discrete-level supply, which modulates an efficient 12-W GaN MMIC *X*-band PA, as shown in Fig. 1. In this approach, the digital baseband signal is generated and predistorted in an FPGA and upconverted to drive modulate the GaN-on-SiC 10-GHz MMIC PA. The FPGA also provides control bits for a 3-b power DAC (pDAC) multilevel

Manuscript received February 24, 2016; revised June 6, 2016, August 29, 2016, and November 7, 2016; accepted November 12, 2016. Date of publication December 16, 2016; date of current version March 3, 2017. This work was supported in part by the Office of Naval Research under Defense Advanced Research Projects Agency within the Microscale Power Conversion Program at University of Colorado, Boulder, under Grant N00014-11-1-0931.

C. Florian, T. Cappello, and D. Niessen are with the Department of Electrical, Electronic and Information Engineering, University of Bologna, 40136 Bologna, Italy (e-mail: corrado.florian@unibo.it).

R. P. Paganelli is with the National Research Council, CNR-IEIIT, 40136 Bologna, Italy.

S. Schafer was with the Department of Electrical, Computer and Energy Engineering, University of Colorado Boulder, Boulder, CO 80303 USA. He is now with Qorvo, Richardson, TX 75080 USA.

Z. Popović is with the Department of Electrical, Computer and Energy Engineering, University of Colorado Boulder, Boulder, CO 80303 USA.

Color versions of one or more of the figures in this paper are available online at http://ieeexplore.ieee.org.

Digital Object Identifier 10.1109/TMTT.2016.2631171

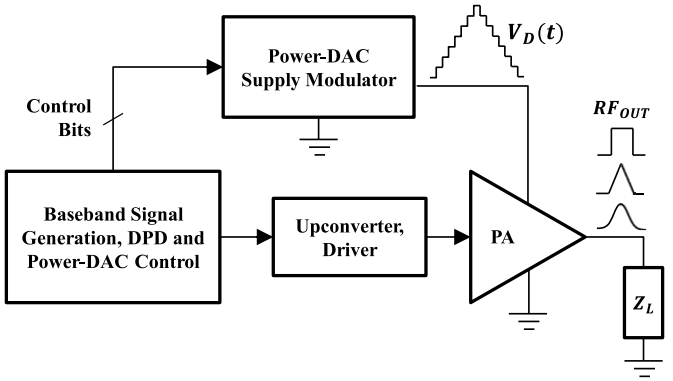

Fig. 1. High-level block diagram of the radar transmitter with a pDAC supply modulator. The digital baseband signal processing provides the signal that is upconverted and drive modulates the PA, as well as the control bits for the pDAC. The pDAC is implemented with GaN-on-Si power devices, while the PA is a GaN-on-SiC MMIC. The digital signal processing includes predistortion.

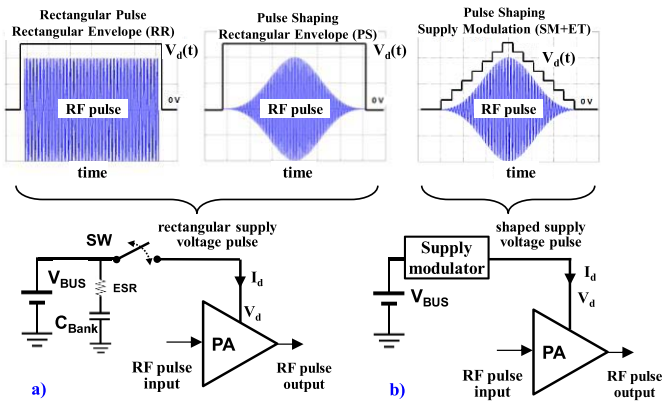

Fig. 2. (a) Pulse waveforms and circuit diagram for constant supply case. (b) Amplitude-modulated pulse waveform with discretized envelope and associated circuit architecture.

dynamic supply, implemented with GaN-on-Si power devices. The pulse shape is fully programmable and can provide not only amplitude modulation of each pulse, but also pulse-to-pulse modulation.

In the work presented here, and in contrast to linear tracking, such as described in [2], the pDAC discretizes the envelope in steps and the linearity is recovered by digital predistortion (DPD) of the RF PA. The switches of the pDAC commutate at only a few kilohertzes, and the nonlinearities are compensated with DPD, allowing for large efficiency increase to over 55% at the X-band.

The multilevel power converter (pDAC) used here as the supply modulator of a radar transmitter was first introduced in [24] for the implementation of an envelope tracking (ET) transmitter at L-band for LTE communication signals with a hybrid LDMOS PA. Here, the pDAC is used as a part of an X-band radar transmitter based on a GaN MMIC PA. The exploitation of the pDAC for this new application enables the synthesis of arbitrary, digitally programmable radar pulse envelope shaping, while maintaining very high composite efficiency. This type of transmitter enables other useful operating modes, such as PWM and pulse-to-pulse modulation.

The remainder of this paper presents the transmitter architecture and measurement setup, detailed in Section II, followed by a brief description of the pDAC multilevel supply modulator and required predistortion in Section III. Section IV presents the design and characterization of the MMIC PA at X-band. In Section V, the results of the transmitter measurements with the pDAC connected to the MMIC PA show that high average overall efficiency can be obtained with simultaneous high dynamic range and spectral confinement. Section VI presents a discussion of other relevant capabilities of this architecture, such as PWM and pulse-to-pulse modulation. Section VII concludes this paper.

II. Transmitter Architecture and Measurement Setup

A common configuration for the power supply of a radar transmitter is shown in Fig. 2(a). The supply voltage V_d of the RF PA is provided by switching ON/OFF the system bus voltage supply V_{BUS}, which is typically generated by a switching power supply. A power switch [SW in Fig. 2(a)] is connected in series between V_{BUS} and the PA bias pad, and a bank of high-Q capacitors (C_{BANK}) is designed to guarantee a limited roll-off of V_d and delivers the PA supply current (I_d) during the pulse. This type of operation is standard for X- and C-band GaAs and GaN MMIC PAs described in [18]–[20]. The PA operates always at peak power-added efficiency (PAE) deep in gain compression and the strong nonlinearities in addition to rectangular pulse spectral spreading generate significant sidebands in the transmitted radar spectrum. When a Gaussian-type pulse is applied to reduce the spectral-domain sidebands, if the supply is kept constant (PS case in the top part of Fig. 2), the efficiency of the PA is greatly reduced.

Fig. 2(b) shows the alternate approach when the same shaping of the RF pulse envelope is also applied through the supply. Here, a supply modulator is used between the system voltage bus and the PA and dynamically maintains the PA at high efficiency by SM.

The supply amplitude-modulated transmitter system setup is shown in more detail in Fig. 3, along with a photograph of the laboratory setup. The vector signal generator and the analyzer are a National Instrument PXIe-5644R VST, which is an FPGA-based instrument used for the generation and analysis of arbitrary digital modulated RF signals, with an analog bandwidth of 80 MHz. The signal is generated in digital baseband and upconverted first to 1 GHz directly within the VST. A second upconversion stage to X-band is performed with a double-balanced diode mixer (Minicircuits ZX05-153MH-S+) and after filtering, amplification is provided by an instrumentation amplifier (Agilent 83020A). Note that any type of digital vector modulation can be applied to the baseband signal prior to upconversion.

In the receiver section, the RF signal is downconverted twice, sampled, and then analyzed in the time domain. At the PA output, the signal is attenuated (50-dB coaxial attenuator), downconverted to 1 GHz by a second mixer, and low-pass filtered before the VST input port. A microstrip image-rejection filter (IMR-F) in the upconversion chain and a coaxial low-pass filter in the downconversion chain were designed in-house. The external LO (Agilent 83650B) is

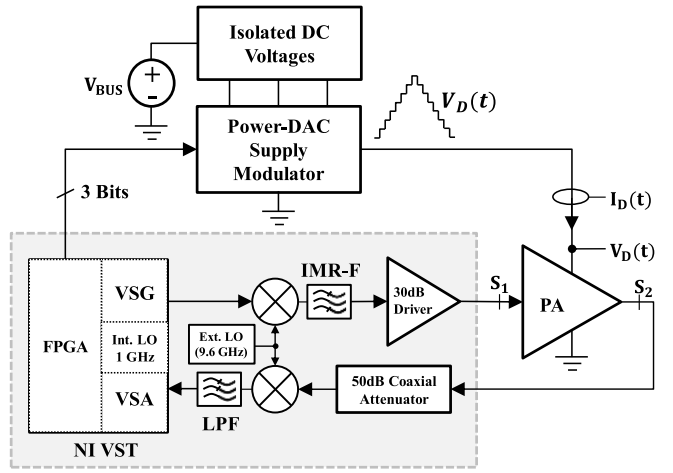

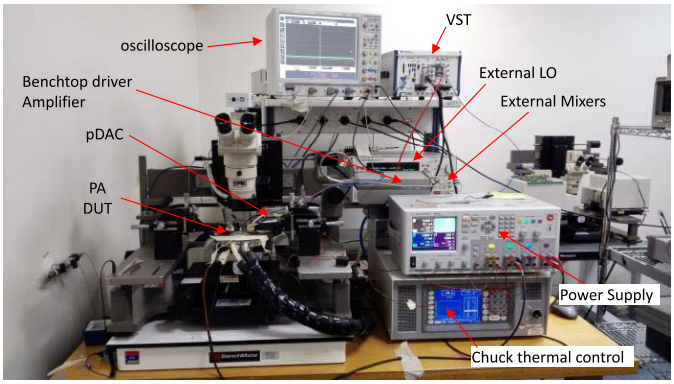

Fig. 3. Block diagram of setup and picture for radar transmitter pulse shaping measurements. Three isolated dc voltages are input to the pDAC, which is controlled from the FPGA in the NI VST 5644R. The mixers are commercial minicircuits devices, and the IMR-F and low-pass filter are specifically designed for this setup.

locked to the same low-frequency reference clock as the internal LO of the VST. The VST stores the I/Q data of the RF signal at the DUT input and output, while the modulated supply voltage $V_d(t)$ and currents $I_d(t)$ of the PA (Fig. 3) are acquired by a digital oscilloscope equipped with wideband voltage and current sensors. The setup is calibrated at the DUT input and output ports, S_1 and S_2 in Fig. 3, corresponding to the GSG probe tips connected at the input and output port of the MMIC PA.

The modulation and DPD associated with a specific pulse shape are implemented in firmware (LabVIEW FPGA VI) and loaded in the instrument FPGA. The firmware also generates digital commands for control of the dynamic bias supply, by comparing the RF signal envelope with the PA bias supply shaping table, which consists of the optimum supply voltage V_d trajectory for PAE maximization [13]. The firmware also regulates time alignment between RF drive and SM paths, which is fundamental to correct SM operation. The FPGA is clocked at 120 MHz, and the control/baseband signal time step is 4.16 ns, due to internal fractional interpolation. The signal flowthrough the test setup can be summarized as follows, referring to Fig. 4.

1) The I/Q signals of the arbitrary shaped pulsed RF waveform $x(n)$ are generated in the VST and their corresponding envelope $|x(n)|$ is calculated in the FPGA.

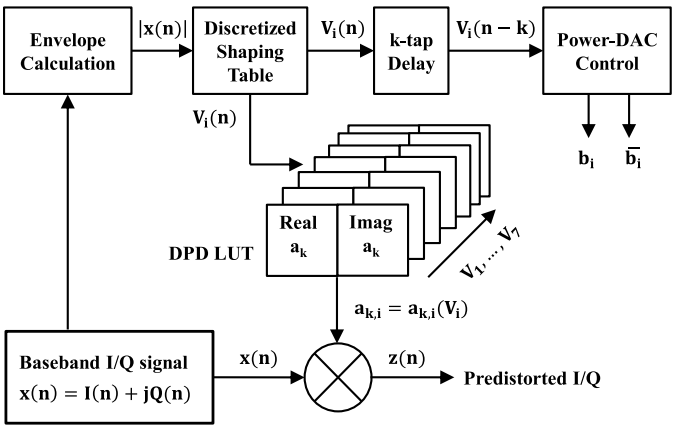

Fig. 4. Generation of the predistorted I/Q and of the pDAC commands in firmware loaded in the FPGA. The top branch shows the envelope signal generation for pDAC control, while the bottom branch describes the generation of the predistorted signal, which is input to a DAC before upconversion.

2) V_i voltage level is selected based on the calculated envelope that maximizes the PAE, according to the PA discretized supply shaping function $V_i = F_D(|x(n)|)$ stored in an LUT in the FPGA. The corresponding digital commands b_i are generated for the pDAC.
3) The value of V_i dictates the complex DPD coefficients $a_{k,i}$ to compensate AM/AM and AM/PM characteristics of the PA at supply level V_i.
4) The DPD coefficients are applied to the input signal to generate the predistorted I/Q, which is then upconverted and input to the PA input, synchronously with the corresponding supply commands b_i.

Referring to Fig. 4, the coefficients $a_{k,i}$ of the seven polynomials corresponding to the seven levels V_i are stored in eight different LUTs. This implementation of the DPD function with multiple LUTs avoids some of the discontinuity problems that could arise with a single predistorter function covering the entire dynamic range of the PA.

The DPD strategy implemented in the setup is in open loop, since there is no adaptation of the DPD coefficients at runtime. However, since the DPD LUTs are implemented in the FPGA of the same instrument that contains the receiver (Fig. 3), a closed-loop DPD can also be implemented, by synthesizing an adaptation algorithm for the DPD coefficients in the FPGA firmware. Such an implementation could be useful to track temperature or aging variations of the PA, or to implement a memory DPD required for higher bandwidth operation (e.g., for wideband radar pulses with pulsewidths lower than 1 μs). For the experiments reported in this paper, with a fixed baseplate temperature ($T_B = 60$ °C), relative short observation time, and pulsewidths in the 1–100-μs range, the memoryless open-loop approach is shown to be sufficient, as will be seen from the measured system-level results in Section V.

III. Power-DAC Supply Modulator and DPD

Multilevel dynamic power supplies demonstrated efficiency improvements in outphasing transmitters [21]–[23]. Typically, one of four supply voltage levels is switched in for a time period that depends on signal statistics. In this paper,

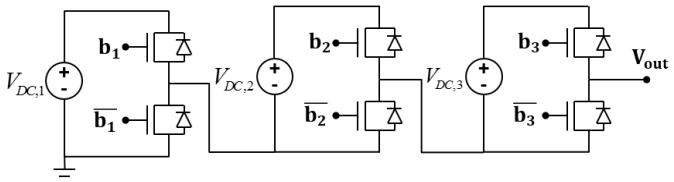

Fig. 5. Three-level pDAC topology with binary-weighted isolated voltage sources.

a different type of multilevel supply is used and we refer to it as a pDAC, because three supply voltages can be combined to give $2^3 = 8$ voltage levels. Because of the discrete nature of the SM, predistortion of the signal becomes a necessity. In this section, the architecture of the pDAC described in detail in [24] is reviewed for completeness, followed by a description of the DPD required for amplitude-modulated radar pulses.

A. Power DAC Supply Modulator

The pDAC shown in Fig. 5 is demonstrated in [24] to effectively modulate an ET hybrid LDMOS S-band PA with 10-MHz LTE and WiFi high PAPR signals. The pDAC features a full power bandwidth larger than 20 MHz and a spurious free dynamic range of about 26.5 dB (measured at 1 MHz).

The modulator is capable of sweeping through its entire voltage dynamic range of 42 V in far less than 1 μs and is thus suitable for tracking the envelope of amplitude-modulated pulsed signals, which are typically 1–100 μs wide in radar applications, The corresponding $V_d(t)$ profile shown in Fig. 2(b) has a discrete staircase shape, produced by the pDAC circuit shown in Fig. 5, composed of three cascaded half-bridge converters, which control three isolated voltage sources ($V_{\mathrm{DC},1}$, $V_{\mathrm{DC},2}$, and $V_{\mathrm{DC},3}$). This converter topology can implement the binary-coded sum of the input voltage sources, with an output waveform resolution of $(2^N - 1)$ levels, compared with N for a standard multilevel converter. The converter output voltage V_{out} is a binary-coded eight-level step waveform (one level is zero) given by

$$V_{\mathrm{out}} = \sum_{i=1}^{3} b_i V_{\mathrm{DC},i} \text{ with } V_{\mathrm{out}}^{\mathrm{MAX}} = V_{\mathrm{DC},1} + V_{\mathrm{DC},2} + V_{\mathrm{DC},3} \tag{1}$$

where b_i is the binary ($b_i = 1, 0$) controlling command of the i-th half bridge cell, generated by the FPGA in Fig. 4. Compared with the common ET approach that combines a PWM switching buck converter with a linear amplifier, the pDAC has advantages in terms of dynamic range, full power bandwidth, and efficiency. The drawback is the limited resolution of the output waveform, which introduces a discretization error in the dynamic supply voltage [$V_{\mathrm{out}}(t) = V_d(t)$], that will also be observed in the PA output signal as distortion. Nonetheless, due to the relatively large number of voltage levels provided by this pDAC topology, the discretization error is limited, and can be compensated by DPD of the RF signal. It is worth noting that the topology of Fig. 6 is modular, and a pDAC with a higher number of bits can be implemented, resulting in finer discretization of the synthesized dynamic

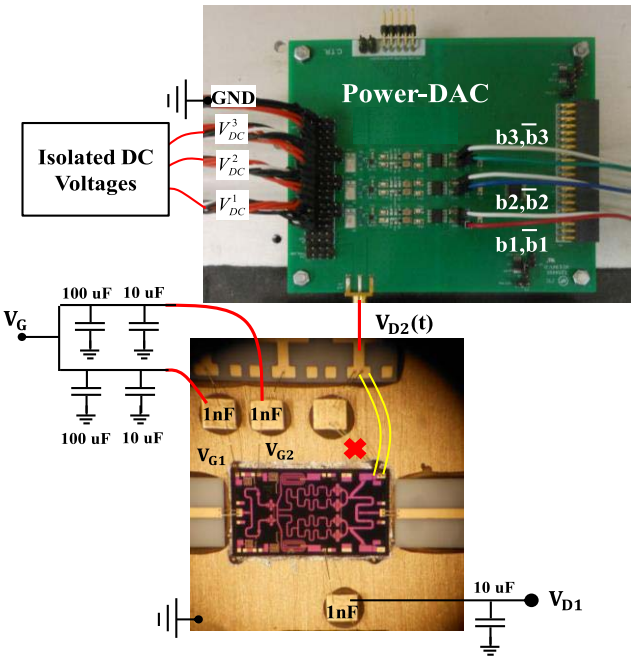

Fig. 6. Photographs of the pDAC board and MMIC PA, with a sketch of the connections of the PA to supplies and to the pDAC. The drain of the second stage amplifier has been directly bonded to the carrier pad.

supply voltage $V_d(t)$. This would increase the average PA efficiency at the expense of an increased number of commutations of the power switches of the pDAC, thus at lower pDAC efficiency. Given this tradeoff for the optimization of the overall transmitter efficiency, a 3-b implementation of the pDAC represents a good compromise, since seven V_d levels are enough to supply modulate a PA with a substantial increase of its operating PAE, while maintaining the pDAC efficiency very high.

B. Digital Predistortion for Pulse Shaping

The predistorter for the linearization of the PA working under SM operation is implemented in open loop with a memoryless polynomial model defined by

$$z(n) = \sum_{k=1}^{K_i} a_{k,i} x(n)|x(n)|^{k-1} \tag{2}$$

$$a_{k,i} = |a_{k,i}| e^{j\angle a_{k,i}} = a_{k,i}(V_i) \quad i = 1 \ldots N \tag{3}$$

$$V_i = \mathcal{F}_D(|x(n)|) \quad i = 1 \ldots N \tag{4}$$

where $x(n)$ is the baseband signal at the PA input before DPD and $z(n)$ is the baseband predistorter output. The complex polynomial coefficients $a_{k,i}$ depend on the instantaneous supply voltage V_i, where the V_i values are selected by the input signal amplitude $|x(n)|$, according to the discretized shaping function F_D. The model coefficients are identified by complex polynomial fitting of the inverse of the PA AM/AM and AM/PM characteristics, with some off-line coefficient optimization, as shown in Section IV. Least-squares fitting of seven complex polynomials, one polynomial for each level V_i, to the measured characteristics is performed.

IV. PA Characterization for Discrete-Level Supply Modulation

The PA is a two-stage MMIC implemented in the Qorvo 0.15-μm GaN-on-SiC HEMT technology.

A similar PA designed in the same process is reported in [25] for tracking OFDM signals with an inefficient linear supply.

The MMIC PA integrated with the pDAC and shown in Fig. 6 is reported here for the first time and is designed for SM with peak efficiency somewhat below the highest level of 20 V. The PA is designed to be stable with no external capacitors on the bias network, since the drain bias network needs to pass broadband signals from the dynamic supply. The first driver stage of the PA is composed of two 8×50 μm devices, while four 10×90 μm devices are combined in the second stage, with a gain greater than 20 dB at 2–3-dB gain compression. The maximum drain supply voltage is $V_D = 20$ V, for a total class-AB quiescent drain current $I_D = 325$ mA (55 mA for the first stage and 270 mA for the second stage).

As seen in Fig. 6, only the second stage of the PA is modulated by the pDAC, while the drain voltage of the first stage is kept fixed at $V_{d1} = 20$ V. Fig. 6 shows the connections between the PA and the pDAC, along with the other drain and gate bias networks. While for V_{G1}, V_{G2}, and V_{d1} bias connections, off-chip bypass capacitors are added to ensure PA stability, no external capacitance is added to the second stage drain pad V_{d2} in order to enable fast modulation of this supply voltage. The only bypass capacitance to this node is provided by the on-chip integrated metal–insulator–metal capacitors, for a total value of 30 pF. The connection between the supply modulator and the PA is kept as short as possible for a total estimated inductance of about 30 nH. The PA is soldered on a large CuMo carrier and the input/output RF pads are accessed with GSG microprobes through short 50-Ω microstrip lines on alumina, wire bonded to the MMIC RF pads. The PA frequency sweep shows a bandwidth from about 9 to 10.5 GHz, with peak efficiency at 9.6 GHz.

The PA was characterized in the setup of Fig. 3 to identify the supply shaping table and the complex polynomial for the DPD. Fig. 7 shows the measured output power at 9.6 GHz versus available source power over a range of final stage drain voltages. The 0–20 V drain voltage interval was discretized with the voltage levels V_i shown in Fig. 7 (inset), synthesized by the pDAC as binary sums of the input voltages $V_{\mathrm{DC},1} = 11.2$ V, $V_{\mathrm{DC},2} = 5.6$ V, and $V_{\mathrm{DC},3} = 3.2$ V.

The measurement results in Figs. 7–9 are performed with a pulsewidth of 50 μs with 10% duty cycle, which are typical values for many types of pulse-compressed radar transmitters (e.g., the ones in [18]–[20]). The AM/AM and AM/PM characterization of the PA is carried out with an amplitude modulated RF pulse, sweeping the entire PA dynamic range for each supply voltage V_i. With this setup, the PA characterization at different supply voltages is carried out in pulsed regime, under thermal conditions very similar to the operating ones.

In Figs. 7 and 8, the measured output power and available power gain of the PA are shown for the different pulsed drain supplies as $V_d = V_i$. The measured PAE is shown in Fig. 9

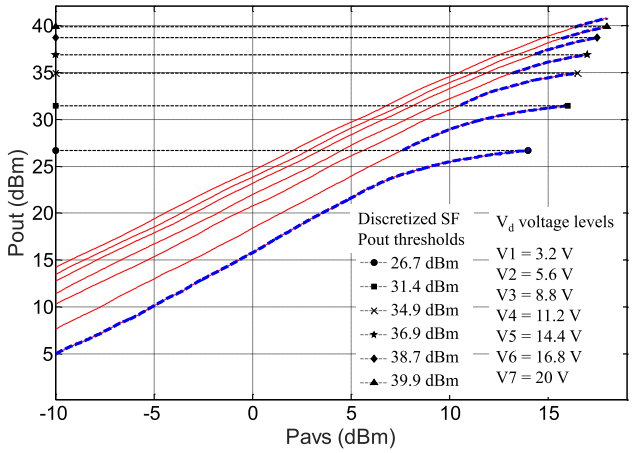

Fig. 7. Measured PA output power for different $V_d = V_i$ values at 9.6 GHz and a gate bias of $V_{G1} = V_{G2} = -2.7$ V for both stages. Bold dashed lines: SM trajectory followed with the selected supply shaping function. Inset: selected discretized supply shaping function is listed as a function of the output power.

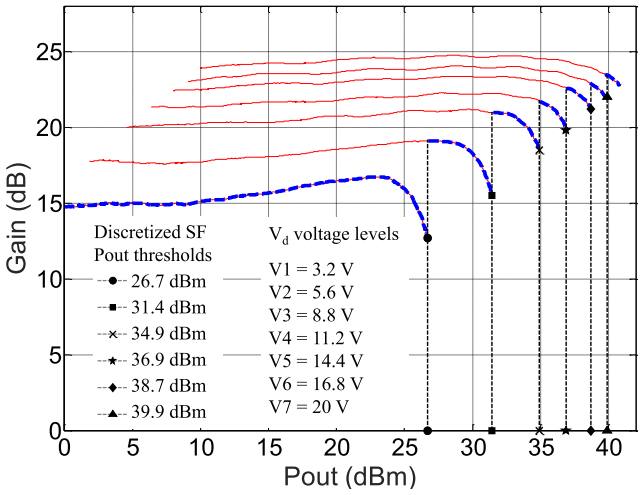

Fig. 8. Measured PA gain at 9.6 GHz for different $V_d = V_i$ values. Bold dashed lines: SM trajectory followed with the selected supply shaping function. Inset: selected discretized supply shaping function is listed as a function of the output power.

where power consumption is calculated from the measured instantaneous values of $V_d(t)$ and $I_d(t)$.

The peak PAE was not reached for the highest voltage levels, due to power limitation of the instrumentation amplifier driver; however, the PA is in more than 2 dB of gain compression even at the $V_d = 20$ V level, as shown in Fig. 8. This characterization shows the following PA peak performance at $V_d = 20$ V: $P_{\mathrm{out}} = 40.7$ dBm, $Gain = 23$ dB, and PAE = 65%.

The selected supply shaping function is represented by P_{out}, PAE, and gain trajectories highlighted with the bold dashed lines in Figs. 7–9. The symbols in the graphs indicate the P_{out} thresholds for V_d level commutation of the discretized shaping table, which is a simple two-column LUT (output or input power versus V_d) stored in the FPGA of the instrument. The shaping table is listed in Figs. 7–9 (insets). In Fig. 8,

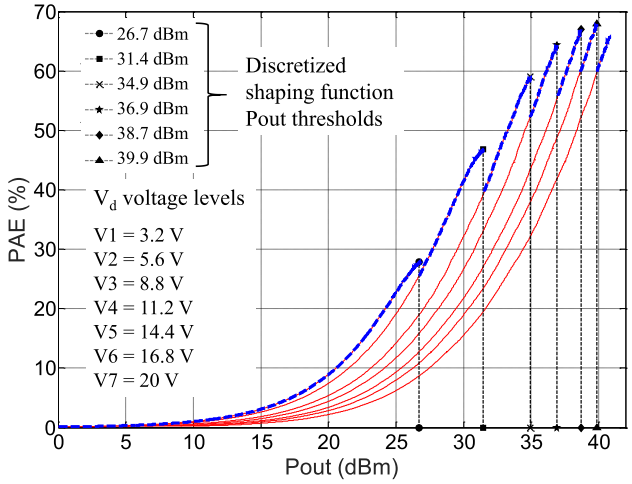

Fig. 9. Measured PA PAE at 9.6 GHz for different $V_d = V_i$ values. Bold dashed lines: SM trajectory followed with selected supply shaping function. Inset: selected discretized supply shaping function is listed as a function of the output power.

the relevant gain variation associated with the selected supply shaping table is shown: this variation (from 15 dB for $V_d = 3.2$ V to 23 dB for $V_d = 20$ V) is due to the variation of the quiescent drain current ($I_{D2} = 48$ mA for $V_d = 3.2$ V and $I_{D2} = 270$ mA for $V_d = 20$ V) and the corresponding change of the input/output impedances, and thus matching characteristics, of the devices in the PA final stage.

The gain steps corresponding to different supply levels and the gain variation within each level need to be compensated by the predistorter, which is designed to linearize the SM PA characteristic to a constant compressed gain of 23 dB, at the maximum output power ($V_d = 20$ V at maximum input power).

Since the PA gain decreases significantly with lower supply voltages (Fig. 8), the predistorter gain needs to provide significant gain expansions to obtain the target constant transmitter gain of 23 dB.

In Fig. 10, the predistorter amplitude and phase characteristics for each voltage level are shown (solid lines), along with the PA AM/AM and AM/PM behavior (bold dashed lines). The DPD amplitude expansion needed for the linearization of the PA gain compression is evident in these plots.

The same information in time domain can be seen in Fig. 11, where the ideal envelope of the RF input signal (bold dashed line) for pulse shaping with a Blackman window is shown along with the actual predistorted envelope for the SM PA linearization (thin solid line).

By observing results in Figs. 8–11, it is seen that the PA output magnitude (thus power and gain) significantly changes with supply level, showing a strong nonlinear behavior of the PA. This indicates that the operating regime cannot be defined as pure ET, since its fundamental definition, given for example in [26], requires that the PA operates almost linearly under supply variation. Since the amplitude sensitivity to supply variation is not 1:1 (see Figs. 10 and 11), the PA is also not operating in EER regime, but rather in a hybrid mode of SM that maximizes efficiency, while the strong linearity is recovered by DPD.

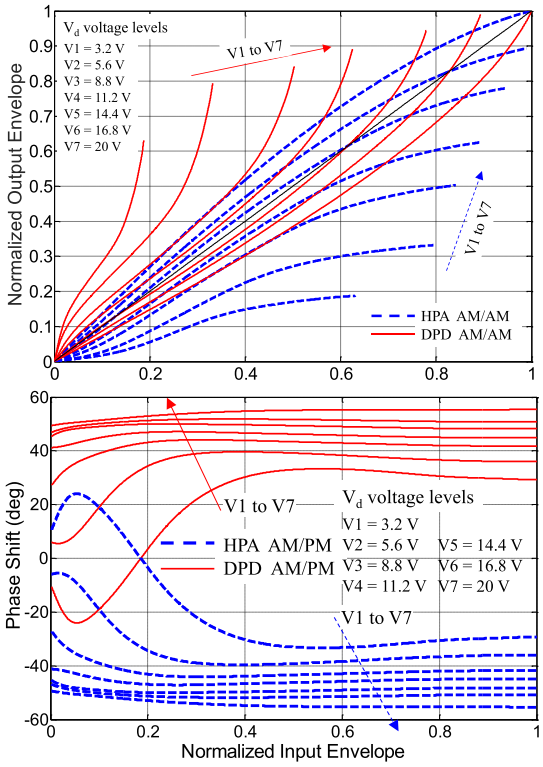

Fig. 10. PA and predistorter AM/AM (top) and AM/PM (bottom) characteristics for each supply voltage level.

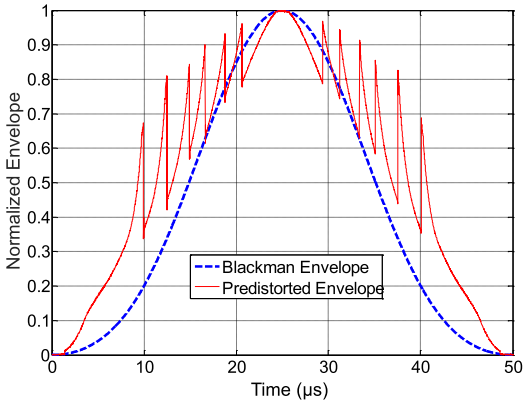

Fig. 11. Comparison between the ideal envelope of the RF input signal and the actual predistorted one for the case of pulse shaping with Blackman window.

V. Transmitter System Tests

The setup of Fig. 3 is used to compare the transmitter performance with different RF pulse shapes and SM regimes. In the standard regime, both the RF envelope and supply voltage are unmodulated rectangular pulses [RR regime of Fig. 2(a)]. Three different windowing functions, triangular, Hanning, and Blackman, are applied to the RF pulse envelope, each one with two different pulsed-supply regimes: rectangular supply pulse [PS regime in Fig. 2(a)] and modulated drain supply [PS + SM regime in Fig. 2(b)]. In the case of PS + SM regime, experiments with and without DPD are also performed and compared. The pulse duration for all the measurements presented in this section is $\tau = 50$ μs, with 10% duty cycle.

TABLE I
PERFORMANCE WITH DIFFERENT PULSE SHAPING STRATEGIES

Pulse Shape Window (PAPR)	Bias supply Modulation	1st sidelobe (dBm)	Power per pulse W (dBm)	PAE (%) PA	p-DAC	tot.
Rectangular	Rectangular pulse	-12.8 dB	11.75 (40.7)	65.0	96	62.4
Blackman (5.17 dB)	Rectangular pulse	-30.2 dB	3.57 (35.52)	37.2	96	35.7
Blackman (5.17 dB)	SM + DPD	-46.0 dB (ideal -58 dB)	3.57 (35.52)	**58.1**	95	55.2
Triangle (4.77 dB)	Rectangular pulse	-28 dB *	3.91 (35.91)	35.1	96	33.4
Triangle (4.77 dB)	SM + DPD	-26.5 dB (ideal -26.5 dB)	3.91 (35.91)	**58.9**	95	55.9
Hanning (4.20 dB)	Rectangular pulse	-24.4 dB	4.40 (36.43)	40.2	96	38.6
Hanning (4.20 dB)	SM+ DPD	-31.5 dB (ideal -31.5 dB)	4.40 (36.43)	**59.3**	95	56.3

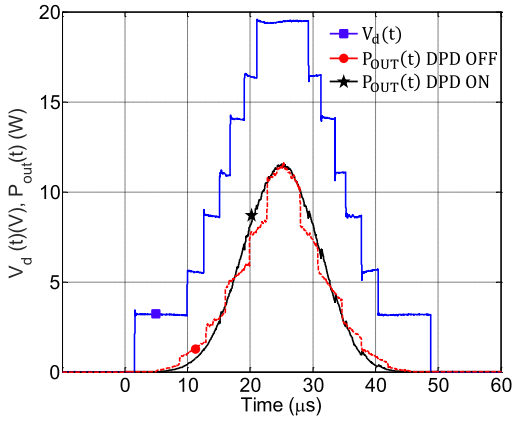

Fig. 12. Measured dynamic supply voltage $V_d(t)$ (blue square) and PA instantaneous output power $P_{\text{out}}(t)$ for SM operation with Blackman window pulse shaping with DPD OFF (red dot) and DPD ON (black star). Gain steps due to the pDAC discrete operation are evident in the instantaneous output power when DPD is OFF, while they are compensated when DPD is applied.

The measured $V_d(t)$ when operating in PS + SM regime with a Blackman window is shown in Fig. 12, along with the PA RF output power. From these measurements, it is obvious that the memoryless polynomial open-loop DPD is effective in linearizing the PA nonlinearity that arises from discretized SM. In Fig. 12, the smooth transitions between the levels in the pulse indicate excellent time alignment between the supply and RF paths achieved during the calibration phase. As observed in [10], a precise time alignment is more important in such a hybrid ET/EER system than in a pure ET transmitter.

Moreover, the voltage ringing associated with transitions in the $V_d(t)$ trace of Fig. 12 and the corresponding transients in the output envelope $[P_{\text{OUT}}(t)]$ are limited in amplitude and duration due to the excellent switching characteristics of the selected GaN-on-Si technology (very low parasitics, see [24]) and the optimization of the connection between the pDAC and the PA.

In order to test spectral confinement, Figs. 13 and 14 show the measured output spectra of the three pulse shaping regimes with different windowing. In each plot of Fig. 14, the output spectrum in SM regime with DPD (RX—bold solid line) is compared with the ideal spectrum of that particular windowing (TX— bold dashed line). The measured spectrum in the conventional RR regime (rectangular— thin dashed line) is also shown for reference.

Finally, in Fig. 13, the spectra obtained with RF pulse shaping and no DPD are compared with the rectangular constant-supply pulse case [PS regime of Fig. 2(a)] and ideal spectra of the corresponding windowing. Even though in this regime the PA operates in strong backoff over most of the pulse duration, the output spectrum is distorted with respect to the ideal one, due to the nonlinearity of the PA toward the peak of the pulse, which increases the sideband level or shifts their position closer to the main lobe. Fig. 14 clearly shows the improvement when DPD is performed, with sidelobes spectra much closer to the ideal ones even in the presence of the more nonlinear and efficient SM regime.

In Table I, the measured performance of the transmitter in the different regimes is compared and summarized. For each regime, the efficiencies of the PA and pDAC are stated separately, along with the total composite efficiency, averaged over the pulse duration in each case. As expected, the maximum PA PAE $= 65\%$ is obtained for constant-envelope rectangular pulses when the PA is always in saturation and operating at peak efficiency. However, in this case, the first spectral sideband is at a high value of -12.8 dBc. With RF pulse shaping alone, and no SM, the PAE drops to 40.2% for Hanning windowing. The application of pulse shaping in conjunction with SM provided by the pDAC restores the PAE to 59.3%, providing an improvement of $+19.1$ PAE points with an associated improvement in suppression of the first spectral sidelobe of 18.7 dB. Similar improvements are observed for the triangular and Blackman pulse shapes, as summarized in Table I.

The very high efficiency provided by the pDAC working as a supply modulator (95%) guarantees that this advantage in terms of PAE of the RF PA is preserved also at the transmitter level, as seen in the last column in Table I.

VI. DISCUSSION

This section discusses some properties of the SM PA system with a pDAC, such as additional functionality to include pulse-to-pulse shaping, as well as possible extensions of the DPD.

These functionalities give to the pDAC-based SM transmitter enhanced flexibility and additional operative modes, compared with other solutions presented in the literature [29].

A. Pulse-to-Pulse Modulation

In [14]–[16], a resonant pulse modulator is presented with good efficiency, but with very limited pulse shape variation.

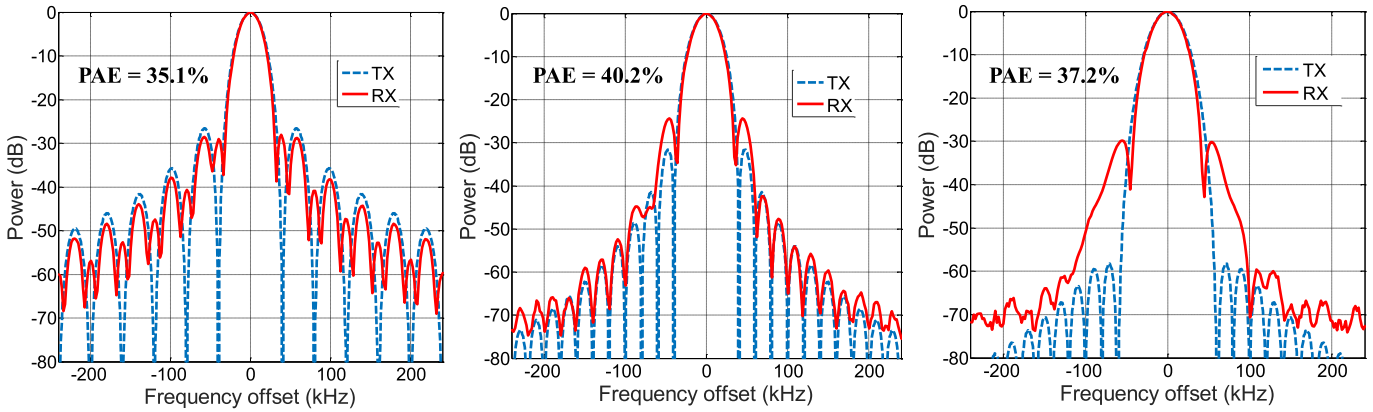

Fig. 13. PA measured normalized output spectrum (RX) without DPD compared with the ideal one (TX) in pulse shaping regimes with unmodulated rectangular supply pulse (rectangular V_d). Triangular (left), Hanning (center), and Blackman (right) pulse shapes are shown.

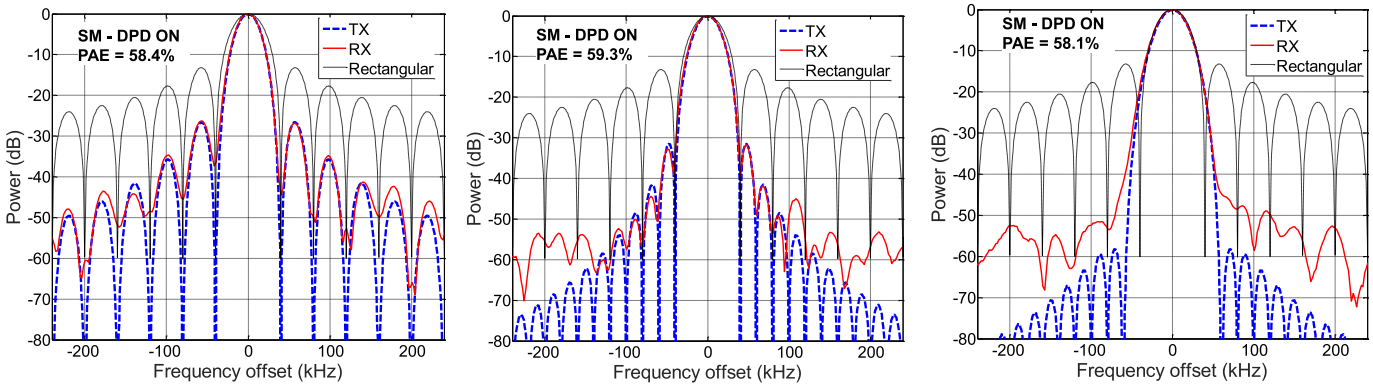

Fig. 14. Comparison between input (TX—ideal) and output spectra (RX) of the PA with triangular (left), Hanning (center), and Blackman (right) pulse shaping in SM regime with the pDAC and DPD applied. The rectangular (RR regime) pulse response is shown for comparison.

In contrast, the approach described in this paper is completely flexible in terms of pulse shape and dynamic range. The $V_d(t)$ trajectory synthesized by the pDAC automatically adapts to the RF pulse shape and amplitude, according to the supply shaping function stored in the FPGA, delivering the radar pulse with the maximum possible efficiency compatible with the V_d range discretization.

It is sometimes advantageous from a system perspective to generate pulse sequences with pulse-to-pulse modulation. Two examples that demonstrate the flexibility are measured using the pDAC supply modulator and shown in Figs. 15 and 16. In the first case, a sequence of four pulses with different shapes, lengths, and peak amplitudes is generated, and in Fig. 15, the normalized envelopes of the pulse sequence are shown at the PA input and output, along with the corresponding $V_d(t)$ synthesized by the pDAC. The different types of shapes and values of length and peak power of the pulses are indicated in Fig. 15 (inset). For each pulse, the setup automatically selects the $V_d(t)$ trajectory that maximizes the PA PAE.

Fig. 16 shows a different case of pulse-to-pulse modulation, which could be used to modify time on target and power on target of a radar on a pulse-to-pulse basis. The pDAC can produce square voltage pulses with the seven different

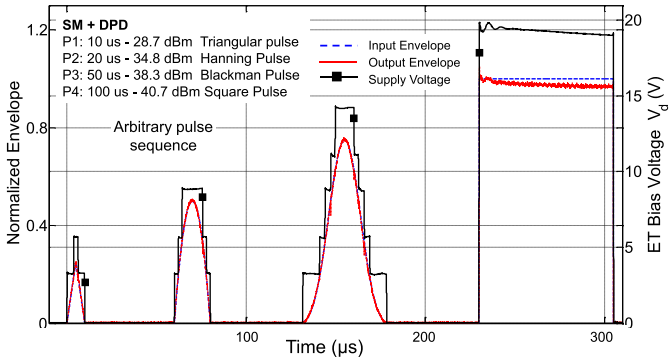

Fig. 15. Arbitrary pulse sequence: triangular, Hanning, Blackman, and square pulse envelopes. The transmitted RF envelope is almost indistinguishable from the input one, due to the DPD correction effect. The corresponding dynamic supply voltage is also shown.

amplitudes described in (1), since $V_{\text{out}} = 0$ V is not used. Table II summarizes the pulse characteristics and the measured PAE and compares them with the performance obtained with constant 0–20 V supply pulses. The advantage in terms of PAE is substantial, since the PA *Vd* is practically optimized for all the different output power levels ranging from 17 to 40.5 dBm.

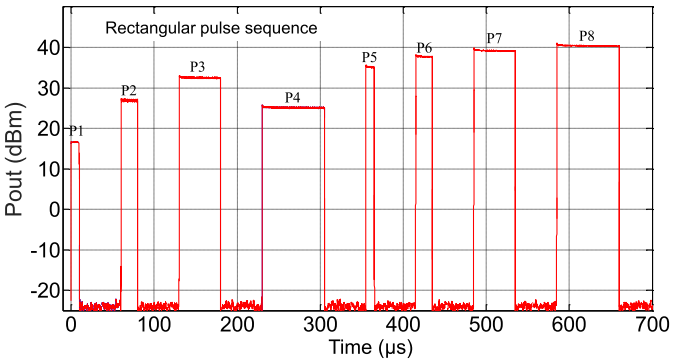

Fig. 16. Instantaneous PA output power for an arbitrary rectangular pulse sequence. Each power level is obtained with an optimal V_d for PAE maximization. No RF power (P_{out}) is present between pulses. The noise floor of the instrument is −25 dBm, when set with reference level and resolution bandwidth for the detection of the pulses with power up to 40 dBm.

TABLE II
PERFORMANCE WITH DIFFERENT RECTANGULAR PULSE AMPLITUDES

Pulse	Width (µs)	Supply Level (V)	Pout (dBm/W)	PAE (%) SM	PAE (%) pulsed Vd = 0-20V
P1	10	3.2	17 / 0.05	5	1
P2	20	5.6	27 / 0.5	27	9
P3	50	8.8	32.5 / 1.78	43	21
P4	75	11.2	35.3 / 3.38	55	32
P5	10	11.2	35.3 / 3.38	55	32
P6	20	14.4	37.6 / 5.75	60	45
P7	50	16.8	39.2 / 8.32	63	55
P8	75	20.0	40.5 / 11.22	66	66

B. Digital Predistortion Extensions

It is worth noting that further improvements in linearization are possible. Some of the distortion is likely due to observed asymmetries between the upside and the downside slopes of the shaped RF pulses, not corrected by the current DPD. This is most probably due to nonlinear trapping effects. We recently demonstrated a double-pulsed technique specifically designed for trapping effect characterization, which shows that memory effects due to trapping can be corrected with appropriate DPD. More details are given in [27].

As described in detail in [24], one of the main characteristics of the pDAC is that, despite being a switching converter, it does not use PWM modulation. This means that a fixed switching frequency is not used, but rather the commutation of the power switches is determined by the instantaneous amplitude of the envelope and by the quantization thresholds. In other words, the switching is adapting to the signal. This allows a minimum switching rate and thus high efficiency. As described in [24], for a periodic full-amplitude signal (i.e., full-amplitude radar pulse for this application), the power switches of the most significant bit commutate one time per period, the switches of the intermediate bit three times per period, and the switches of the least significant bit seven times per period. Since the pulse repetition frequency of the tested radar signals 500 μs, the commutation frequencies of the power switches are 2, 6, and 14 kHz, respectively. Note that all these contributions, and several of their harmonics, fall within the measurement span of 250 kHz of Fig. 14. Thus, the main contributions of the switching spurious noise of the pDAC are included in the measurement span of Fig. 14 and appear to be negligible.

As previously observed in the comments of Fig. 12, the transition between voltage levels of the pDAC introduces additional distortion (envelope transients at the PA output). DPD with additional LUTs, specifically designed for compensation of switched supply voltage transients, was demonstrated in [28] to improve the spectral properties in such cases, and can be implemented in the FPGA predistorter in a straightforward manner. Further improvement of the linearity of the output spectra is expected, especially for pulse shapes with demanding characteristics (i.e., very high sidelobe suppression), for example, Gaussian pulses with a high PAR, in addition to the Hanning and Blackman pulses in Fig. 14.

VII. CONCLUSION

In summary, the application of a 3-b pDAC as a supply modulator for radar pulse shaping is demonstrated for the first time. The approach is shown to give very high flexibility and the state-of-the-art performance in terms of transmitter composite PAE (55%) with low spectral out-of-band regrowth. The GaN MMIC PA used in the transmitter demonstrates the state-of-the-art performance with 65% peak efficiency at the X-band for 12-W output power and with $>$20-dB gain at 2–3-dB gain compression. The pDAC implemented with off-the-shelf GaN on Si devices operates at a very high efficiency of 95–96% efficiency.

Spectral confinement of radar signals with improved efficiency was tested for different RF pulse shape windowing and detailed comparisons with unmodulated pulsed regimes with a basic pulsed bias supply are presented. The improvement in spectral properties is enabled by pulse shaping combined with appropriate DPD.

In this paper, we considered only amplitude modulation but it is possible to add both linear and nonlinear frequency chirp. Due to the capability of the VST to generate arbitrary digitally modulated baseband signals, with some modification of the firmware, the setup can be programmed for the test of the transmitter with both AM and FM modulated (i.e., chirped) driving signals.

The capability of the supply modulator to synthesize arbitrary supply trajectories with efficiency greater than 95% and the adopted DPD strategy results in a very high flexibility in the implementation of arbitrary pulse sequences with variable sequence order, pulse shape, length, and peak amplitude, for advanced radar transmitters.

ACKNOWLEDGMENT

The authors would like to thank National Instruments for invaluable support with instrumentation and support, especially Dr. J. Truchard, F. Signorini, Dr. M. V. Bossche, P. Webb, and Dr. T. Inoue. They would also like to thank Qorvo for collaboration during MMIC fabrication. T. Cappello would like to thank the support through a graduate fellowship at the DEI Department of the University of Bologna.

REFERENCES

[1] M. I. Skolnik, *Radar Handbook*. New York, NY, USA: McGraw-Hill, 2008, ch. 11.

[2] G. van der Bent *et al.*, "A 10 watt S-band MMIC power amplifier with integrated 100 MHz switch-mode power supply and control circuitry for active electronically scanned arrays," *IEEE J. Solid-State Circuits*, vol. 48, no. 10, pp. 2285–2295, Oct. 2013.

[3] D. A. Garren, M. K. Osborn, A. C. Odom, J. S. Goldstein, S. U. Pillai, and J. R. Guerci, "Enhanced target detection and identification via optimised radar transmission pulse shape," *Proc. Inst. Electr. Eng.—Radar, Sonar Navigat.*, vol. 148, no. 3, pp. 130–138, Jun. 2001.

[4] *Weather Radar Technology Beyond NEXRAD* (Committee (within the The Nat. Acad. Sci., Eng. Med.) Board Atmospher. Sci. Climate, Div. Earth Life Studies, Nat. Res. Council), Nat. Acad. Sci., Eng., Med., Washington, DC, USA, 2002.

[5] C. Baylis, M. Fellows, L. Cohen, and R. J. Marks, "Solving the spectrum crisis: Intelligent, reconfigurable microwave transmitter amplifiers for cognitive radar," *IEEE Microw. Mag.*, vol. 15, no. 5, pp. 94–107, Jul. 2014.

[6] R. Chen and B. Cantrell, "Highly bandlimited radar signals," in *Proc. IEEE Radar Conf.*, Apr. 2002, pp. 220–226.

[7] J. de Graaf, H. Faust, J. Alatishe, and S. Talapatra, "Generation of spectrally confined transmitted radar waveforms: Experimental results," in *Proc. IEEE Conf. Radar*, Apr. 2006, pp. 76–83.

[8] E. McCune, *Dynamic Power Supply Transmitters*. Cambridge, U.K.: Cambridge Univ., 2015, chs. 5–6.

[9] G. Hanington, P. M. Asbeck, P.-F. Chen, and L. E. Larson, "High-efficiency power amplifier using dynamic power-supply voltage for CDMA applications," *IEEE Trans. Microw. Theory Techn.*, vol. 47, no. 8, pp. 1471–1476, Aug. 1999.

[10] F. Wang, A. H. Yang, D. F. Kimball, L. E. Larson, and P. M. Asbeck, "Design of wide-bandwidth envelope-tracking power amplifiers for OFDM applications," *IEEE Trans. Microw. Theory Techn.*, vol. 53, no. 4, pp. 1244–1255, Apr. 2005.

[11] D. F. Kimball *et al.*, "High-efficiency envelope-tracking W-CDMA base-station amplifier using GaN HFETs," *IEEE Trans. Microw. Theory Techn.*, vol. 54, no. 11, pp. 3848–3856, Nov. 2006.

[12] J. Hoversten, S. Schafer, M. Roberg, M. Norris, D. Maksimovic, and Z. Popovic, "Codesign of PA, supply, and signal processing for linear supply-modulated RF transmitters," *IEEE Trans. Microw. Theory Techn.*, vol. 60, no. 6, pp. 2010–2020, Jun. 2012.

[13] K. Bumman, M. Junghwan, and K. Ildu, "Efficiently amplified," *IEEE Microw. Mag.*, vol. 11, no. 5, pp. 87–100, Aug. 2010.

[14] M. Roberg, M. Rodriguez, D. Maksimovic, and Z. Popovic, "Efficient and linear amplification of spectrally confined pulsed AM radar signals," *IEEE Microw. Wireless Compon. Lett.*, vol. 22, no. 6, pp. 279–281, Jun. 2012.

[15] M. Rodriguez, M. Roberg, A. Zai, E. Alarcon, Z. Popovic, and D. Maksimovic, "Resonant pulse-shaping power supply for radar transmitters," *IEEE Trans. Power Electron.*, vol. 29, no. 2, pp. 707–718, Feb. 2014.

[16] A. Zai, M. Pinto, M. Coffey, and Z. Popović, "Supply-modulated radar transmitters with amplitude-modulated pulses," *IEEE Trans. Microw. Theory Techn.*, vol. 63, no. 9, pp. 2953–2964, Sep. 2015.

[17] L. R. Kahn, "Single-sideband transmission by envelope elimination and restoration," *Proc. IRE*, vol. 40, no. 7, pp. 803–806, Jul. 1952.

[18] C. Florian, R. P. Paganelli, and J. A. Lonac, "12-W *X*-band MMIC HPA and driver amplifiers in InGaP-GaAs HBT technology for space SAR T/R modules," *IEEE Trans. Microw. Theory Techn.*, vol. 60, no. 6, pp. 1805–1816, Jun. 2012.

[19] C. Florian, R. Cignani, D. Niessen, and A. Santarelli, "A C-band AlGaN-GaN MMIC HPA for SAR," *IEEE Microw. Wireless Compon. Lett.*, vol. 22, no. 9, pp. 471–473, Sep. 2012.

[20] C. Florian, R. Cignani, A. Santarelli, and F. Filicori, "Design of 40-W AlGaN/GaN MMIC high power amplifiers for *C*-band SAR applications," *IEEE Trans. Microw. Theory Techn.*, vol. 61, no. 12, pp. 4492–4504, Dec. 2013.

[21] P. A. Godoy, S. W. Chung, T. W. Barton, D. J. Perreault, and J. L. Dawson, "A highly efficient 1.95-GHz, 18-W asymmetric multilevel outphasing transmitter for wideband applications," in *IEEE MTT-S Int. Microw. Symp. Dig.*, Jun. 2011, pp. 1–4.

[22] P. A. Godoy, S. Chung, T. W. Barton, D. J. Perreault, and J. L. Dawson, "A 2.4-GHz, 27-dBm asymmetric multilevel outphasing power amplifier in 65-nm CMOS," *IEEE J. Solid-State Circuits*, vol. 47, no. 10, pp. 2372–2384, Oct. 2012.

[23] J. Hur, O. Lee, K. Kim, K. Lim, and J. Laskar, "Highly efficient uneven multi-level LINC transmitter," *Electron. Lett.*, vol. 45, no. 16, p. 837, Jul. 2009.

[24] C. Florian, T. Cappello, R. P. Paganelli, D. Niessen, and F. Filicori, "Envelope tracking of an RF high power amplifier with an 8-level digitally controlled GaN-on-Si supply modulator," *IEEE Trans. Microw. Theory Techn.*, vol. 63, no. 8, pp. 2589–2602, Aug. 2015.

[25] A. Zai, L. Dongxue, S. Schafer, and Z. Popovic, "High-efficiency X-band MMIC GaN power amplifiers with supply modulation," in *IEEE MTT-S Int. Microw. Symp. Dig.*, Jun. 2014, pp. 1–4.

[26] F. H. Raab *et al.*, "Power amplifiers and transmitters for RF and microwave," *IEEE Trans. Microw. Theory Techn.*, vol. 50, no. 3, pp. 814–826, Mar. 2002.

[27] C. Florian, D. Niessen, T. Cappello, A. Santarelli, F. Filicori, and Z. Popovic, "Pre-pulsing characterization of GaN pas with dynamic supply," in *IEEE MTT-S Int. Microw. Symp. Dig.*, San Francisco, CA, USA, May 2016, pp. 1–4.

[28] N. Wolff, W. Heinrich, and O. Bengtsson, "A novel model for digital predistortion of discrete level supply-modulated RF power amplifiers," *IEEE Microw. Wireless Compon. Lett.*, vol. 26, no. 2, pp. 146–148, Feb. 2016.

[29] A. Zai, C. Florian, T. Cappello, and Z. Popovic, "Efficient power amplifiers for amplitude-tapered pulses with improved spectral confinement," in *IEEE MTT-S Int. Microw. Symp. Dig.*, San Francisco, CA, USA, May 2016, pp. 1–4.

Corrado Florian (S'02–M'04) received the Ph.D. degree in electronics from the University of Bologna, Bologna, Italy, in 2004.

Since 2006, he has been a Research Associate with the Department of Electrical, Electronic and Information Engineering, University of Bologna, where he is currently a Lecturer of power electronics and RF electronics courses. His current research interests include RF and microwave circuit, power electronics, microwave, and power device characterization and modeling.

Tommaso Cappello (GS'14) is currently pursuing the Ph.D. degree in electronics with the University of Bologna, Bologna, Italy.

He is currently with the Department of Electrical, Electronic and Information Engineering, University of Bologna. His current research interests include power electronics, digital signal processing/field programmable gate array-based control design, and RF electronics.

Daniel Niessen (S'05–M'13) received the Ph.D. degree in electronics, computer science, and telecommunications from the University of Bologna, Bologna, Italy, in 2013.

In 2012, he was a Visiting Researcher with the Chalmers University of Technology, Gothenburg, Sweden. Since 2013, he has been a Research Fellow with the Department of Electrical, Electronic and Information Engineering, University of Bologna. His current research interests include nonlinear characterization and modeling of electron devices and systems (with special focus on GaN technology), microwave circuit design and linearization techniques.

Rudi Paolo Paganelli received the Ph.D. degree in electronics from the University of Bologna, Bologna, Italy, in 2002.

Since 2002, he has been a Research Fellow with the CNR-IEIIT and an Assistant Professor of the course on power electronics with the University of Bologna. His current research interests include electron device modeling, microwave circuit, and power electronics.

Scott Schafer (S'10) received the B.S. degree in engineering physics from the Colorado School of Mines, Golden, CO, USA, in 2010, and the Ph.D. degree from the University of Colorado Boulder, Boulder, CO, USA, in 2015.

He is currently with Qorvo, Richardson, TX, USA. His current research interests include millimeter-wave near-field probing, envelope tracking for power amplifiers, and GaN monolithic microwave integrated circuit microwave PA design.

Dr. Schafer was a recipient of the Russell Hayes Graduate Fellowship at the University of Colorado Boulder.

Zoya Popović (S'86–M'90–SM'99–F'02) received the Dipl.Ing. degree from the University of Belgrade, Belgrade, Serbia, in 1985, and the Ph.D. degree from the California Institute of Technology, Pasadena, CA, USA, in 1990.

Since 1990, she has been with the University of Colorado Boulder, Boulder, CO, USA, where she is currently a Distinguished Professor and holds the Hudson Moore Jr. Endowed Chair with the Department of Electrical, Computer and Energy Engineering. Since 1991, she has been supervised 56 Ph.D. students. She was a Visiting Professor with the Technical University of Munich, Munich, Germany, in 2001, and with the École nationale supérieure de l'aéronautique et de l'espace, Toulouse, France, 2014. She was a Distinguished Research Lecturer with the University of Colorado, in 2015. She currently leads a group of 16 doctoral students and two post-doctoral fellows. Her current research interests include high-efficiency transmitters for radar and communication, low-noise and broadband microwave and millimeter-wave circuits, antenna arrays, wireless powering for batteryless sensors, and medical application of microwaves such as core-body thermometry and traveling-wave MRI.

Dr. Popović was a recipient of the 1993 and 2006 IEEE Microwave Theory and Techniques Society (MTT-S) Microwave Prizes for the best journal papers. She received the 1996 URSI Issac Koga Gold Medal and was the NSF White House Presidential Faculty Fellow in 1993. She was a recipient of the 2000 Humboldt Research Award for Senior U.S. Scientists from the German Alexander von Humboldt Stiftung. She was elected a Foreign Member of the Serbian Academy of Sciences and Arts in 2006. She was also a recipient of the 2001 Hewlett-Packard/American Society for Engineering Education Terman Medal for combined teaching and research excellence. In 2013, she was the IEEE MTT Distinguished Educator.